

The Role of Oxygen in Ionic Liquid Gating on 2D Cr₂Ge₂Te₆: a Non-Oxide Material

Yangyang Chen^{1,2†}, Wenyu Xing^{1,2†}, Xirui Wang^{1,2†}, Bowen Shen^{1,2}, Wei Yuan^{1,2}, Tang Su^{1,2},
Yang Ma^{1,2}, Yunyan Yao^{1,2}, Jiangnan Zhong^{1,2}, Yu Yun^{1,2}, X. C. Xie^{1,2}, Shuang Jia^{1,2*}, and Wei
Han^{1,2*}

¹International Center for Quantum Materials, School of Physics, Peking University, Beijing
100871, P. R. China

²Collaborative Innovation Center of Quantum Matter, Beijing 100871, P. R. China

†These authors contributed equally to the work

*Correspondence to: weihan@pku.edu.cn (W.H.); gwljiahuang@pku.edu.cn (S. J.)

KEYWORDS: Ionic liquid gating, Oxygen, Two-dimensional Ferromagnetic Cr₂Ge₂Te₆,
Electrostatic field effect, Channel resistance, Iontronics

ABSTRACT

Ionic liquid gating can markedly modulate the materials' carrier density so as to induce metallization, superconductivity, and quantum phase transitions. One of the main issues is whether the mechanism of ionic liquid gating is an electrostatic field effect or an electrochemical effect, especially for oxide materials. Recent observation of the suppression of the ionic liquid gate-induced metallization in the presence of oxygen for oxide materials suggests the electrochemical effect. However, in more general scenarios, the role of oxygen in ionic liquid gating effect is still unclear. Here, we perform the ionic liquid gating experiments on a non-oxide

material: two-dimensional ferromagnetic $\text{Cr}_2\text{Ge}_2\text{Te}_6$. Our results demonstrate that despite the large increase of the gate leakage current in the presence of oxygen, the oxygen does not affect the ionic liquid gating effect ($< 5\%$ difference), which suggests the electrostatic field effect as the mechanism on non-oxide materials. Moreover, our results show that the ionic liquid gating is more effective on the modulation of the channel resistances compared to the back gating across the 300 nm thick SiO_2 .

1. INTRODUCTION

Ionic liquid gating has been widely used to induce many interesting physical properties by tuning the carrier density higher than 10^{14} cm^{-2} arising from the extremely large electric field on one material.¹⁻³ For example, superconductivity has been induced by ionic liquid gating in a large variety of materials including SrTiO_3 , KTaO_3 , and $\text{La}_{2-x}\text{Sr}_x\text{CuO}_4$, quasi-two dimensional layered ZrNCl , and two-dimensional (2D) transition metal dichalcogenides, etc.⁴⁻¹² Besides, the magnetic properties and magnetic phase transition have also been achieved via ionic liquid gating.¹³⁻¹⁶ Despite these intensive progresses, whether the gating mechanism is an electrostatic field effect or an electrochemical effect is still under debate, especially for oxide materials, such as VO_2 and SrTiO_3 . For the ionic liquid gating induced metallization in VO_2 , Nakano et al attributed the mechanism to the carrier doping via electrostatic field effect,¹⁷ while Jeong et al attributed it to the oxygen vacancy formation, which is an electrical chemical process.¹⁸ For SrTiO_3 ,^{4, 19-21} Gallagher et al found that the ionic liquid gating can induce the metallization of SrTiO_3 protected by a chemically inert hexagonal boron nitride, which supports the electrostatic field effect,²⁰

while Li et al demonstrated the strong suppression of the metallization in the presence of oxygen, which supports the oxygen vacancy as the major cause.²¹

One of the main experimental proofs to support the electrochemical effect as the mechanism for the metallization in oxide materials is the strong suppression of the ionic liquid gating effect in the presence of oxygen.^{18,21-24} However, in more general scenarios, the role of oxygen in ionic liquid gating effect, i.e. on a non-oxide material, is still not clear. In this letter, we report the negligible role of oxygen in the ionic liquid gating effect on 2D Cr₂Ge₂Te₆ (CGT), a non-oxide material. The ionic liquid gating provides a more powerful tool to tune the channel resistance than the back gate through 300 nm thick SiO₂. In the presence of oxygen gas, despite the large increase of the gate leakage current, the effect of the ionic liquid gating on the channel resistance is not affected. A tiny difference (< 5 %) of the gating response is observed. Our experimental results indicate that oxygen gas plays a negligible role in the ionic liquid gating. The results are important for future application of ionic liquid and the emerging field of iontronics.

2. MATERIALS AND METHODS

2.1 Materials. 2D CGT flakes have been shown to be an intrinsically ferromagnetic 2D material recently.^{25, 26} To study the ionic liquid gating effect on the 2D CGT device, we synthesized the CGT single crystal by the flux method,^{27, 28} and exfoliated the 2D CGT flakes on the SiO₂ (300 nm) / Si substrates mechanically using the scotch tape method.^{25, 26, 29, 30} The devices are fabricated using standard e-beam lithography and the metallic contacts are made of ~ 80 nm Pt grown by magnetic sputtering.

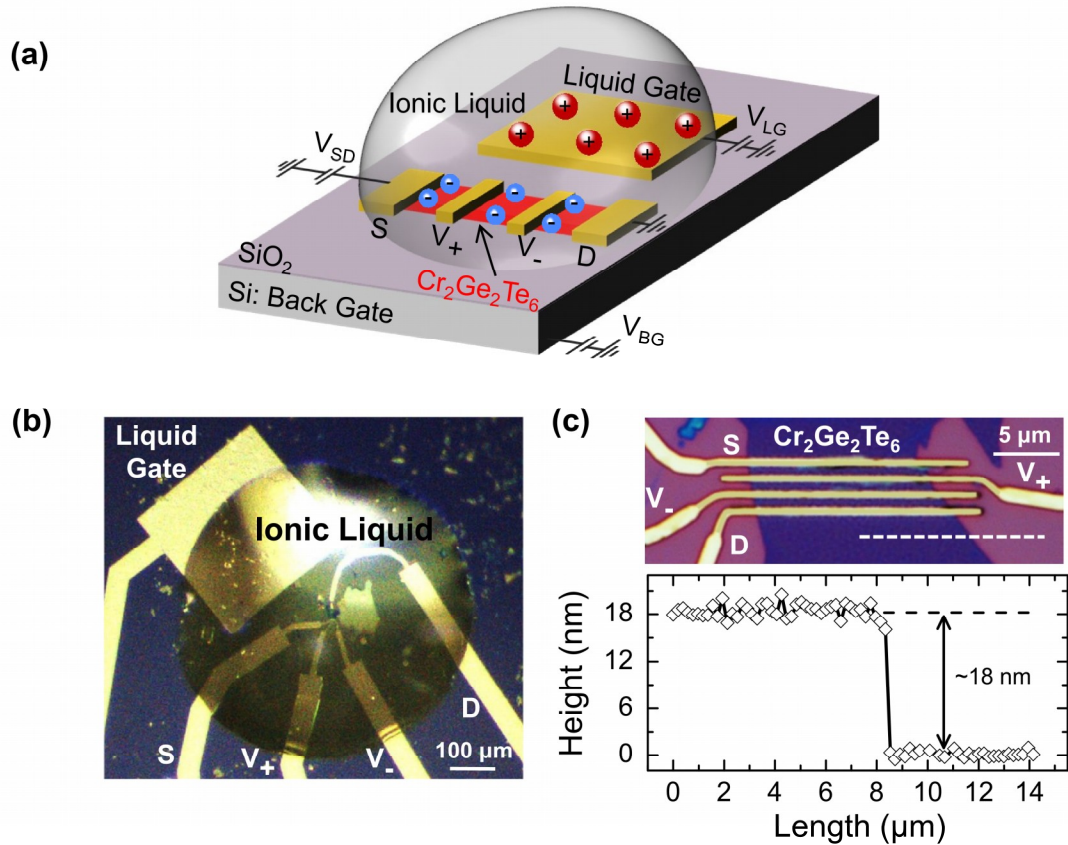


Figure 1. Ionic liquid gating on 2D CGT devices. (a) Schematic of the device geometry and the measurement configuration. (b) Optical image of a typical CGT device covered with a droplet of HMIM-TFSI ionic liquid. (c) The magnified image of this CGT device (top) and the CGT thickness of ~ 18 nm determined from the atomic force microscopy (bottom). Four Pt electrodes are contacted to the 2D CGT flake.

2.2 Device fabrication and measurements. The details of the synthesis of the CGT single crystals and fabrication of 2D CGT devices can be found in our earlier reports.^{26, 28} A lateral gate electrode made of Pt (area: $350 \mu\text{m} \times 350 \mu\text{m}$) is fabricated near the device as the ionic liquid gate during the same step fabricating the Pt electrical contacts. Prior to the ionic liquid gating experiment, the fabricated devices and ionic liquids are annealed in vacuum ($\sim 8 \times 10^{-5}$ Pa) at ~ 100 °C for more than 12 hours to remove the water.^{18, 21} A ~ 100 nL droplet of ionic liquid, 1-

hexyl-3-methyl-imidazolium bis(trifluoromethylsulfonyl)imide (HMIM-TFSI), is put on the device and the lateral Pt gate electrode, as illustrated in Figures 1 (a) and (b). Then the 2D CGT devices covered with ionic liquid are quickly loaded into a vacuum system ($\sim 4 \times 10^{-5}$ Pa) for the electrical measurements. Since the CGT devices are fabricated on top of an oxidized Si substrate (300 nm SiO₂), the back gate voltage is applied between the highly doped Si and the devices across the 300 nm thick insulating SiO₂.

During the gating measurement, a Keithley 2400 source meter is used to apply the liquid gate voltage (V_{LG}) and to record the gate leakage current (I_{LG}), and another Keithley 2400 source meter is used to apply the back gate voltage (V_{BG}) across the 300 nm insulating SiO₂. The channel resistance (R_{XX}) is obtained from the voltage measured by a Keithley 2002 voltage meter on the center two electrodes (V_+ and V_-) and the current (I_{SD}) measured by another Keithley 2400 source meter that provides a constant voltage (V_{SD}) of 0.2 V during the whole measurement.

3. RESULTS AND DISCUSSION

3.1 Ionic liquid gating results. All the data we present in this letter are taken from the same device (Figure 1 (b) and (c)) to make a fair comparison of the ionic liquid gating response to various oxygen environments. Similar results are obtained on more than 10 CGT devices with various CGT thicknesses. The response of the liquid gating to oxygen gas is the same for all devices that oxygen does not affect the liquid gating on CGT, a non-oxide material. All the measurements on the typical device are performed for at least three times. The thickness of this 2D CGT is ~ 18 nm determined by atomic force microscopy (Figure 1 (c)), and the fabricated 2D CGT device has a channel width of ~ 13.5 μm and a channel length of ~ 1 μm . The ionic liquid

gating response of the 2D CGT device in vacuum is measured at first. Figures 2 (a-c) show the time dependence results of V_{LG} , I_{LG} , and R_{XX} of the 2D CGT device measured at 300 K. The V_{LG} is steadily ramped from 0 V to -0.5 V (orange), -1.0 V (blue), -1.5 V (purple), -2 V (green), -2.5 V (red) with a ramping rate of 10 mV/s, which results in the increase of I_{LG} and decrease of R_{XX} . The ionic liquid gate voltage dependence of R_{XX} is showed in Figure 2 (d). The hysteretic behavior of R_{XX} vs. V_{LG} is usually observed in ionic liquid gating studies.^{3, 17, 18, 21} Figure 2 (e) summarizes the R_{XX} obtained from the corresponding I-V curves (Inset of Figure 2 (e)) as a function of the ionic liquid gate voltages at 300 K. It is clearly seen that the ionic liquid gating provides a large modulation of channel resistance: R_{XX} at $V_{LG} = -2.5$ V is ~ 30 times smaller than the value at $V_{LG} = 0$ V.

3.2 Ionic liquid gate vs. back gate. The gating responses from the ionic liquid gate and the back gate across ~ 300 nm thick insulating SiO_2 are compared on this device. Figure 3 (a) shows the gating responses for both the back gate voltages (V_{BG}) with V_{LG} at 0 V (black stars) and V_{LG} with V_{BG} at 0 V (red balls), and Figure 3 (b) shows the color mapping plot of R_{XX} as a function of V_{BG} and V_{LG} . It is clearly showed from Figures 3 (a) and 3 (b) that the liquid gating effect on the CGT is more effective on electric field modulation of the channel resistances compared to the back gating through 300 nm thick SiO_2 . This observation is consistent with previous reports on the dual gating responses in graphene and MoS_2 devices.^{3, 8}

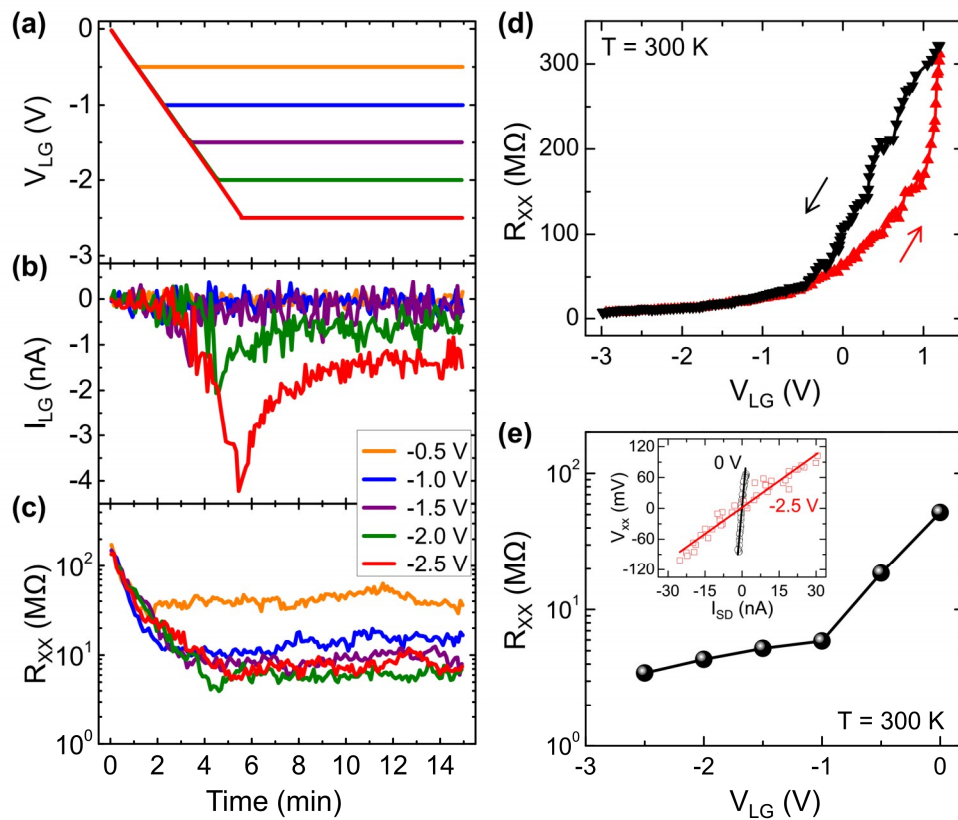


Figure 2. Ionic liquid gating response of 2D CGT devices in vacuum. (a-c) Time dependence of V_{LG} , I_{LG} , and R_{XX} under different gate voltage from -0.5 to -2.5 V. (d) Hysteretic curve of R_{XX} during the ramping measurement of V_{LG} between 1.2 and -3.0 V. (e) R_{XX} vs. V_{LG} . R_{XX} is obtained from the current-voltage measurements (inset).

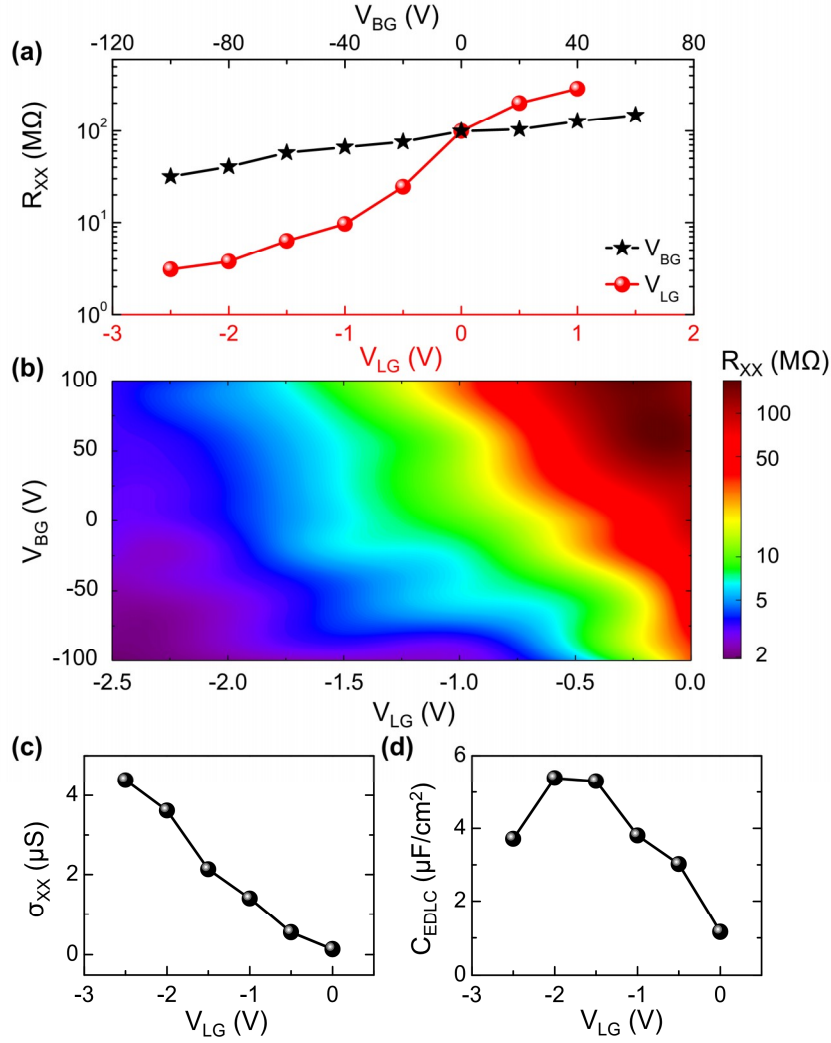


Figure 3. Dual gate response of the 2D CGT device. (a) R_{XX} as a function of V_{BG} (black stars) and V_{LG} (red balls). (b) Color mapping of the R_{XX} as a function of the V_{BG} (y axis) and V_{LG} (x axis). (c-d) The channel sheet conductance (σ_{XX}) and ionic liquid capacitance of (C_{EDLC}) as a function of V_{LG} .

Based on the gate dependence of the channel conductance (Figure 3(c)), the ionic liquid capacitance (C_{EDLC}) can be calculated using the following equation:^{3, 31}

$$C_{EDLC} = \frac{d\sigma/dV_{LG}}{d\sigma/dV_{BG}} \frac{\mu_{BG}}{\mu_{LG}} C_{BG} \quad (1)$$

where μ_{BG} and μ_{LG} are the electron field mobility, and C_{BG} is the capacitance for the 300 nm SiO_2 . Using $C_{\text{BG}} = 11.5 \text{ nF/cm}^2$ from previous studies, the values of C_{EDL} are in the range between 1.2 and 5.4 $\mu\text{F/cm}^2$ as shown in the Figure 3 (d). The obtained values of C_{EDL} are in good agreement with the effective gate capacitances reported in previous ionic liquid gating measurements (1 ~ 20 $\mu\text{F/cm}^2$) on graphene and MoS_2 .^{3, 31} Moreover, based on the gate-tuned channel resistance, the estimated electron field mobility is $\sim 0.4 \text{ cm}^{-2}/\text{V} \cdot \text{s}$, which is much lower compared to semiconducting 2D materials, including black phosphorus and MoS_2 .³²⁻³⁴ This low mobility might be related to defects scattering in the CGT flakes, which needs further experimental and theoretical studies.

3.3 Role of oxygen in Ionic liquid gating. Next, we focus on the study of role of oxygen in ionic liquid gating by performing the gating experiments while systematically varying the oxygen pressure via a high precision leak valve and a turbo pump. Prior to leaking high purity oxygen gas ($\geq 99.999\%$) into the vacuum system, we thoroughly pump out and purge the gas line with the oxygen gas to remove any water or impurity gas. Figure 4 (a) shows the ionic liquid gate voltage dependence of R_{XX} in vacuum ($\sim 4 \times 10^{-5} \text{ Pa}$), 10 Pa, and 50 Pa oxygen environments, and Figure 4 (b) shows the corresponding gate leakage current as a function of ionic liquid gate voltage. Obviously, the leakage current is much larger in the presence of oxygen, which is consistent with previous reports on the ionic liquid gating experiments on VO_2 and SrTiO_3 in oxygen gas.^{18, 21} However, the ionic liquid gate voltage dependences of R_{XX} are almost identical under different oxygen partial pressures. The difference of the gating effect is less than 5 % between in vacuum and 50 Pa O_2 . These results show that the ionic liquid gating of 2D CGT does not affected by the oxygen gas, despite the presence of oxygen largely increases the gate leakage current.

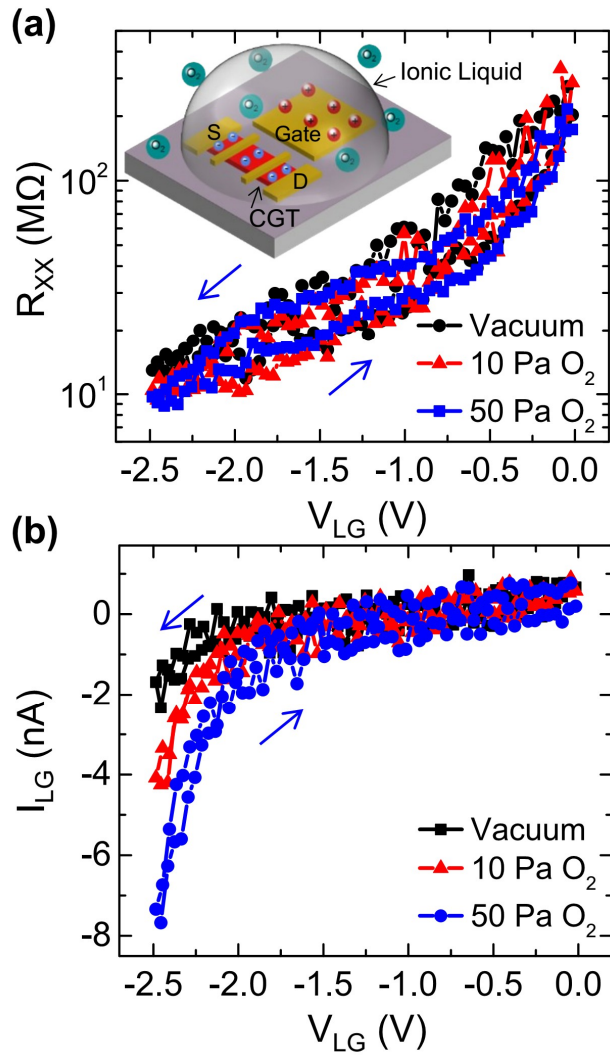


Figure 4. Ionic liquid gate measurements of the 2D CGT device in vacuum and oxygen. Hysteretic loops of R_{XX} (a) and I_{LG} (b) as a function of V_{LG} in vacuum (4×10^{-5} Pa, black) and different oxygen pressure (10 Pa, red and 50 Pa, blue). Inset of (a): Schematic of ionic liquid gating on 2D CGT in the presence of oxygen gas.

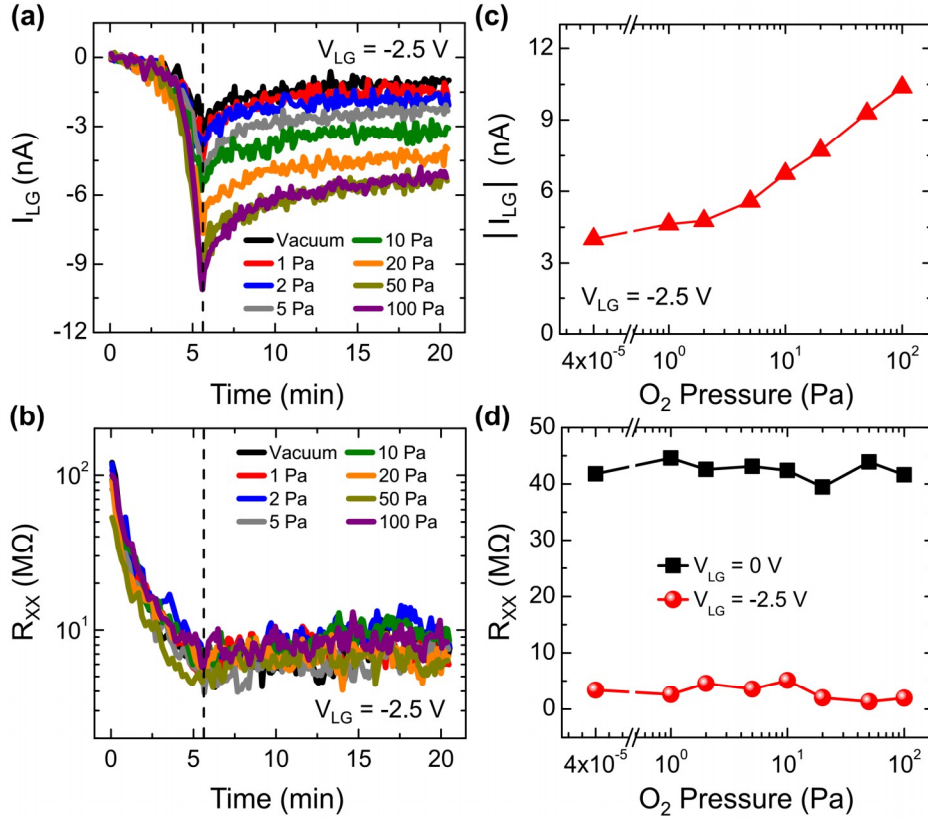


Figure 5. The role of oxygen in the liquid gating on the 2D CGT device. (a-b) Time dependence of I_{LG} (a) and R_{XX} (b) at $V_{LG} = -2.5$ V in vacuum (4×10^{-5} Pa) and different oxygen environments (oxygen pressure from 1 to 100 Pa). (c) The maximum of leakage current vs. oxygen pressure with V_{LG} at -2.5 V. (d) R_{XX} vs. oxygen pressure with V_{LG} at 0 V and -2.5 V.

Then, we systematically change the oxygen pressure and study its effect on the gate leakage current and R_{XX} as a function of time under the same ionic liquid gate voltage of -2.5 V. Figure 5 (a) and 5 (b) show the detailed time dependence of gate leakage current and R_{XX} in various oxygen gas environments (vacuum and 1, 2, 5, 10, 20, 50, and 100 Pa oxygen gas). A larger leakage current corresponds to a higher oxygen pressure, which is consistent with previous reports.^{18, 21} The maximum leakage current as a function of the oxygen pressure for $V_{LG} = -2.5$ V is summarized in Figure 5 (c). The gate leakage current monotonically increases as the oxygen

pressure increases. Figure 5 (d) shows the summary of R_{XX} at $V_{LG} = 0$ V and $V_{LG} = -2.5$ V as a function of the oxygen pressure. Despite the large enhancement of the gate leakage current, the gating response of the channel resistances is not affected. These experimental results further support previous studies that the ionic liquid gate induced metallization in various oxide materials (TiO_2 , VO_2 , WO_3 , $SrTiO_3$, etc) arises from the oxygen vacancies.^{18, 21-23, 35}

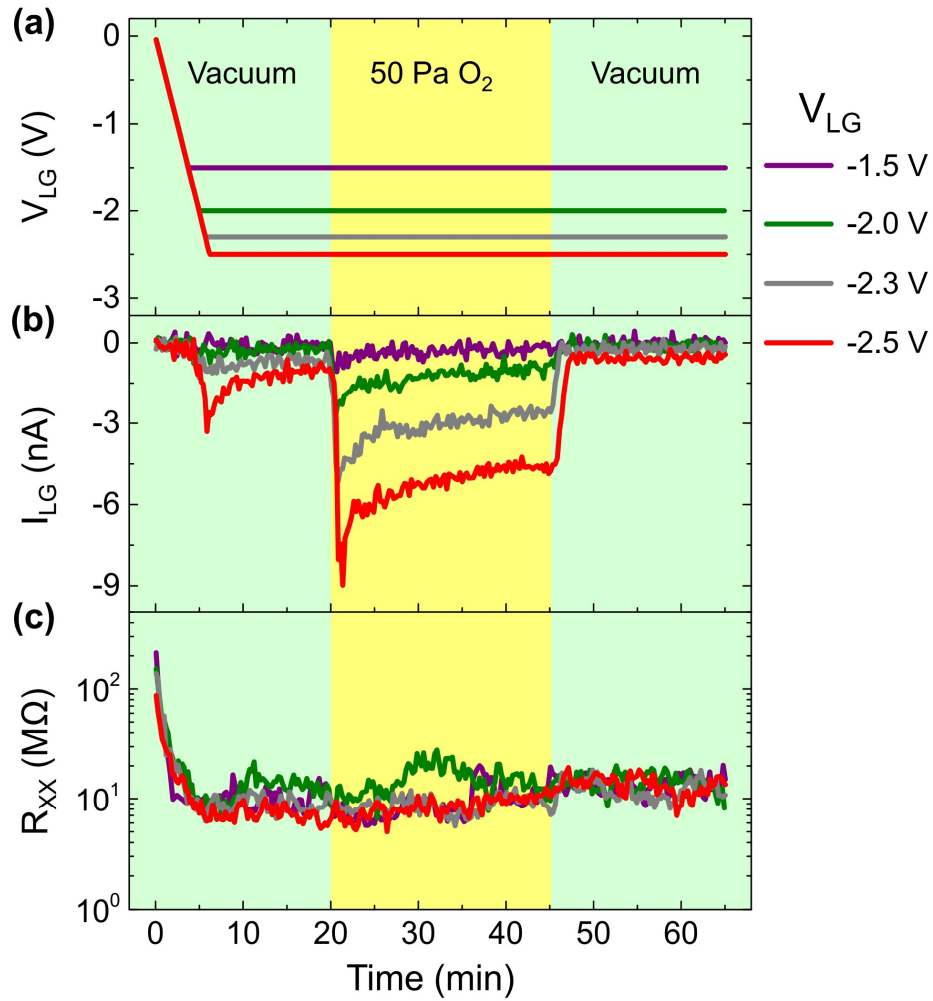


Figure 6. The role of oxygen in the liquid gating on the 2D CGT device. Time dependence of V_{LG} (a), I_{LG} (b), and R_{XX} (c) in the cycle of vacuum, oxygen injection, and pump-out back to vacuum for $V_{LG} = -1.5$, -2.0 , -2.3 , and -2.5 V, respectively.

To further identify the negligible role of oxygen in the ionic liquid gating on the 2D CGT device, we measure the response of the leakage current and R_{XX} as the oxygen pressure varies during the gating experiments under the constant ionic liquid gate voltages of -1.5, -2.0, -2.3, and -2.5 V, respectively. As shown in Figure 6, for each ionic liquid gate voltage, 50 Pa oxygen is injected to the vacuum chamber for ~ 25 minutes and then pumped out. As soon as the 50 Pa oxygen is introduced, the leakage current abruptly increases and then decays slowly. When the oxygen gas is pumped out at ~ 45 minutes and the pressure quickly goes back to $\sim 4 \times 10^{-5}$ Pa, the gate leakage current dramatically decreases to the value prior to the injection of oxygen gas. The average resistances at $V_{LG} = -2.5$ V are ~ 9.0 M Ω before oxygen is injected (from 5 to 20 minutes), ~ 8.7 M Ω when the oxygen is maintained in the chamber (from 20 to 45 minutes), and ~ 10 M Ω when the oxygen is pumped out (from 45 to 60 minutes). Compared to the initial resistance at $V_{LG} = 0$ V (~ 140 M Ω), the variation of the gating response is negligible ($< 5\%$). These results further prove that oxygen does not affect the ionic liquid gating on the 2D CGT device, but only affect the gate leakage current.

4. CONCLUSIONS

In summary, we have performed the ionic liquid gating experiments on the 2D ferromagnetic CGT flakes, and have observed a much larger gating effect compared to the back gating across 300 nm thick SiO₂. Most importantly, we have demonstrated that role of oxygen in the ionic liquid gating on 2D CGT is negligible despite the large enhancement of gate leakage current in the presence of oxygen gas up to 100 Pa. These results support that the ionic liquid gating effect on Cr₂Ge₂Te₆, a non-oxide material, is an electrostatic effect. Our work demonstrates that ionic

liquid gating can also be used in oxygen environment for non-oxide systems, which will be helpful for future applications of ionic liquid gating in the field of iontronics.¹

AUTHOR INFORMATION

Corresponding Authors

*Email: weihan@pku.edu.cn (W.H.); gwljiashuang@pku.edu.cn (S. J.)

Author Contributions

The manuscript was written through contributions of all authors. All authors have given approval to the final version of the manuscript.

†These authors contributed equally.

Funding Sources

National Basic Research Programs of China and National Natural Science Foundation of China

Competing interests

The authors declare no competing financial interests.

ACKNOWLEDGMENTS

We acknowledge the financial support from National Basic Research Programs of China (973 program Grant Nos. 2015CB921104, 2014CB920902, 2013CB921901 and 2014CB239302) and National Natural Science Foundation of China (NSFC Grant No. 11574006). W.H. also acknowledges the support by the 1000 Talents Program for Young Scientists of China.

REFERENCES:

1. Bisri, S. Z.; Shimizu, S.; Nakano, M.; Iwasa, Y. Endeavor of Iontronics: From Fundamentals to Applications of Ion-Controlled Electronics. *Adv. Mater.* **2017**, *29*, 1607054.
2. Yuan, H.; Shimotani, H.; Tsukazaki, A.; Ohtomo, A.; Kawasaki, M.; Iwasa, Y. High-Density Carrier Accumulation in ZnO Field-Effect Transistors Gated by Electric Double Layers of Ionic Liquids. *Adv. Func. Mater.* **2009**, *19*, (7), 1046-1053.
3. Ye, J.; Craciun, M. F.; Koshino, M.; Russo, S.; Inoue, S.; Yuan, H.; Shimotani, H.; Morpurgo, A. F.; Iwasa, Y. Accessing the transport properties of graphene and its multilayers at high carrier density. *Proc. Natl. Acad. Sci. U.S.A.* **2011**, *108*, (32), 13002-13006.
4. Ueno, K.; Nakamura, S.; Shimotani, H.; Ohtomo, A.; Kimura, N.; Nojima, T.; Aoki, H.; Iwasa, Y.; Kawasaki, M. Electric-field-induced superconductivity in an insulator. *Nat. Mater.* **2008**, *7*, (11), 855-858.
5. Ueno, K.; Nakamura, S.; Shimotani, H.; Yuan, H. T.; Kimura, N.; Nojima, T.; Aoki, H.; Iwasa, Y.; Kawasaki, M. Discovery of superconductivity in KTaO₃ by electrostatic carrier doping. *Nat. Nanotechnol.* **2011**, *6*, (7), 408-412.
6. Bollinger, A. T.; Dubuis, G.; Yoon, J.; Pavuna, D.; Misewich, J.; Bozovic, I. Superconductor-insulator transition in La_{2-x}Sr_xCuO₄ at the pair quantum resistance. *Nature* **2011**, *472*, (7344), 458-460.
7. Ye, J. T.; Inoue, S.; Kobayashi, K.; Kasahara, Y.; Yuan, H. T.; Shimotani, H.; Iwasa, Y. Liquid-gated interface superconductivity on an atomically flat film. *Nat. Mater.* **2010**, *9*, (2), 125-128.
8. Ye, J. T.; Zhang, Y. J.; Akashi, R.; Bahramy, M. S.; Arita, R.; Iwasa, Y. Superconducting Dome in a Gate-Tuned Band Insulator. *Science* **2012**, *338*, (6111), 1193-1196.
9. Saito, Y.; Nakamura, Y.; Bahramy, M. S.; Kohama, Y.; Ye, J.; Kasahara, Y.; Nakagawa, Y.; Onga, M.; Tokunaga, M.; Nojima, T.; Yanase, Y.; Iwasa, Y. Superconductivity protected by spin-valley locking in ion-gated MoS₂. *Nat. Phys.* **2016**, *12*, (2), 144-149.
10. Yu, Y.; Yang, F.; Lu, X. F.; Yan, Y. J.; ChoYong, H.; Ma, L.; Niu, X.; Kim, S.; Son, Y.-W.; Feng, D.; Li, S.; Cheong, S.-W.; Chen, X. H.; Zhang, Y. Gate-tunable phase transitions in thin flakes of 1T-TaS₂. *Nat. Nanotech.* **2015**, *10*, (3), 270-276.
11. Li, L. J.; O'Farrell, E. C. T.; Loh, K. P.; Eda, G.; Ozyilmaz, B.; Neto, A. H. C. Controlling many-body states by the electric-field effect in a two-dimensional material. *Nature* **2016**, *534*, (7607), 1-2.
12. Yu, S.; Tsutomu, N.; Yoshihiro, I. Gate-induced superconductivity in two-dimensional atomic crystals. *Supercond. Sci. Technol.* **2016**, *29*, (9), 093001.
13. Yamada, Y.; Ueno, K.; Fukumura, T.; Yuan, H. T.; Shimotani, H.; Iwasa, Y.; Gu, L.; Tsukimoto, S.; Ikuhara, Y.; Kawasaki, M. Electrically Induced Ferromagnetism at Room Temperature in Cobalt-Doped Titanium Dioxide. *Science* **2011**, *332*, 1065.
14. Weisheit, M.; Fähler, S.; Marty, A.; Souche, Y.; Poinignon, C.; Givord, D. Electric Field-Induced Modification of Magnetism in Thin-Film Ferromagnets. *Science* **2007**, *315*, (5810), 349-351.

15. Hatano, T.; Ogimoto, Y.; Ogawa, N.; Nakano, M.; Ono, S.; Tomioka, Y.; Miyano, K.; Iwasa, Y.; Tokura, Y. Gate Control of Electronic Phases in a Quarter-Filled Manganite. *Scientific Reports* **2013**, 3, 2904.
16. Lu, N.; Zhang, P.; Zhang, Q.; Qiao, R.; He, Q.; Li, H.-B.; Wang, Y.; Guo, J.; Zhang, D.; Duan, Z.; Li, Z.; Wang, M.; Yang, S.; Yan, M.; Arenholz, E.; Zhou, S.; Yang, W.; Gu, L.; Nan, C.-W.; Wu, J.; Tokura, Y.; Yu, P. Electric-field control of tri-state phase transformation with a selective dual-ion switch. *Nature* **2017**, 546, (7656), 124-128.
17. Nakano, M.; Shibuya, K.; Okuyama, D.; Hatano, T.; Ono, S.; Kawasaki, M.; Iwasa, Y.; Tokura, Y. Collective bulk carrier delocalization driven by electrostatic surface charge accumulation. *Nature* **2012**, 487, (7408), 459-462.
18. Jeong, J.; Aetukuri, N.; Graf, T.; Schladt, T. D.; Samant, M. G.; Parkin, S. S. P. Suppression of Metal-Insulator Transition in VO₂ by Electric Field-Induced Oxygen Vacancy Formation. *Science* **2013**, 339, (6126), 1402.
19. Lee, M.; Williams, J. R.; Zhang, S.; Frisbie, C. D.; Goldhaber-Gordon, D. Electrolyte Gate-Controlled Kondo Effect in SrTiO₃. *Phys. Rev. Lett.* **2011**, 107, (25), 256601.
20. Gallagher, P.; Lee, M.; Petach, T. A.; Stanwyck, S. W.; Williams, J. R.; Watanabe, K.; Taniguchi, T.; Goldhaber-Gordon, D. A high-mobility electronic system at an electrolyte-gated oxide surface. *Nat. Commun.* **2015**, 6, 6437.
21. Li, M.; Han, W.; Jiang, X.; Jeong, J.; Samant, M. G.; Parkin, S. S. P. Suppression of Ionic Liquid Gate-Induced Metallization of SrTiO₃(001) by Oxygen. *Nano Letters* **2013**, 13, (10), 4675-4678.
22. Schladt, T. D.; Graf, T.; Aetukuri, N. B.; Li, M.; Fantini, A.; Jiang, X.; Samant, M. G.; Parkin, S. S. P. Crystal-Facet-Dependent Metallization in Electrolyte-Gated Rutile TiO₂ Single Crystals. *ACS Nano* **2013**, 7, (9), 8074-8081.
23. Altendorf, S. G.; Jeong, J.; Passarello, D.; Aetukuri, N. B.; Samant, M. G.; Parkin, S. S. P. Facet-Independent Electric-Field-Induced Volume Metallization of Tungsten Trioxide Films. *Adv. Mater.* **2016**, 28, (26), 5284-5292.
24. Xu, P.; Han, W.; Rice, P. M.; Jeong, J.; Samant, M. G.; Mohseni, K.; Meyerheim, H. L.; Ostanin, S.; Maznichenko, I. V.; Mertig, I.; Gross, E. K. U.; Ernst, A.; Parkin, S. S. P. Reversible Formation of 2D Electron Gas at the LaFeO₃/SrTiO₃ Interface via Control of Oxygen Vacancies. *Advanced Materials* **2017**, 1604447-1/8.
25. Gong, C.; Li, L.; Li, Z.; Ji, H.; Stern, A.; Xia, Y.; Cao, T.; Bao, W.; Wang, C.; Wang, Y.; Qiu, Z. Q.; Cava, R. J.; Louie, S. G.; Xia, J.; Zhang, X. Discovery of intrinsic ferromagnetism in two-dimensional van der Waals crystals. *Nature* **2017**, 546, 265-269.
26. Xing, W.; Chen, Y.; Odenthal, P. M.; Zhang, X.; Yuan, W.; Su, T.; Ong, Q.; Wang, T.; Zhong, J.; Jia, S.; Xie, X. C.; Li, Y.; Han, W. Electric field effect in multilayer Cr₂Ge₂Te₆: a ferromagnetic 2D material. *2D Materials* **2017**, 4, (2), 024009.
27. Ji, H.; Stokes, R. A.; Alegria, L. D.; Blomberg, E. C.; Tanatar, M. A.; Reijnders, A.; Schoop, L. M.; Liang, T.; Prozorov, R.; Burch, K. S.; Ong, N. P.; Petta, J. R.; Cava, R. J. A

- ferromagnetic insulating substrate for the epitaxial growth of topological insulators. *J. Appl. Phys.* **2013**, 114, (11), 114907.
28. Zhang, X.; Zhao, Y.; Song, Q.; Jia, S.; Shi, J.; Han, W. Magnetic anisotropy of the single-crystalline ferromagnetic insulator Cr₂Ge₂Te₆. *Japan. J. Appl. Phys.* **2016**, 55, (3), 033001.
 29. Novoselov, K. S.; Jiang, D.; Schedin, F.; Booth, T. J.; Khotkevich, V. V.; Morozov, S. V.; Geim, A. K. Two-dimensional atomic crystals. *Proc. Natl. Acad. Sci. USA* **2005**, 102, 10451.
 30. Yao, T.; Mason, J. G.; Huiwen, J.; Cava, R. J.; Kenneth, S. B. Magneto-elastic coupling in a potential ferromagnetic 2D atomic crystal. *2D Materials* **2016**, 3, (2), 025035.
 31. Uesugi, E.; Goto, H.; Eguchi, R.; Fujiwara, A.; Kubozono, Y. Electric double-layer capacitance between an ionic liquid and few-layer graphene. *Sci. Rep.* **2013**, 3.
 32. Li, L.; Yu, Y.; Ye, G. J.; Ge, Q.; Ou, X.; Wu, H.; Feng, D.; Chen, X. H.; Zhang, Y. Black phosphorus field-effect transistors. *Nat. Nanotech.* **2014**, 9, (5), 372-377.
 33. Liu, H.; Neal, A. T.; Zhu, Z.; Luo, Z.; Xu, X.; Tománek, D.; Ye, P. D. Phosphorene: An Unexplored 2D Semiconductor with a High Hole Mobility. *ACS Nano* **2014**, 8, 4033-4041.
 34. Radisavljevic, B.; Radenovic, A.; Brivio, J.; Giacometti, V.; Kis, A. Single-layer MoS₂ transistors. *Nat. Nanotech.* **2011**, 6, (3), 147-150.
 35. Passarello, D.; Altendorf, S. G.; Jeong, J.; Samant, M. G.; Parkin, S. S. P. Metallization of Epitaxial VO₂ Films by Ionic Liquid Gating through Initially Insulating TiO₂ Layers. *Nano Letters* **2016**, 16, (9), 5475-5481.

TOC Graphic

